Nuclear Instruments and Methods in Physics Research A 636 (2011) S118–S124

Contents lists available at ScienceDirect

Nuclear Instruments and Methods in Physics Research A

journal homepage: www.elsevier.com/locate/nima

Optimization of surface structures in n-in-p silicon sensors using TCAD simulation

Y. Unno [a,*], Y. Ikegami [a], T. Kohriki [a], S. Terada [a], K. Hara [b], K. Yamamura [c], S. Kamada [c]

[a] Institute of Particle and Nuclear Study, High Energy Accelerator Research Organization (KEK), Tsukuba, Ibaraki 305-0801, Japan
[b] The Institute of Pure and Applied Sciences, University of Tsukuba, Tsukuba, Ibaraki 305-8571, Japan
[c] Solid State Division, Hamamatsu Photonics Co. Ltd., Hamamatsu, Shizuoka 435-0051, Japan

ARTICLE INFO

Available online 28 April 2010

Keywords:
Silicon detectors
Microstrip
Semiconductor device simulation
Radiation tolerant
Strip isolation

ABSTRACT

In order to develop a novel n-in-p radiation-tolerant silicon microstrip sensor with a p-stop structure, surface structures are systematically analyzed for variations in the width, position, and multiplicity of p-stops. With the help of technology CAD (TCAD) simulation, three dynamics are quantitatively investigated: the dependence of the electric potential of the p-stops on the width of the p-stops, the similarity between the electric potential of multiple p-stops, which therefore function more like a single large p-stop, and the correlation between the electric potential of the p-stops and the electric field strength in various configurations. The understanding of the electric potential of p-stops and the maximum electric field strength provides a guideline for reducing the electric field at the implant edges and thus for designing a p-stop structure for very-high-voltage operation.

© 2010 Elsevier B.V. All rights reserved.

1. Introduction

A silicon semiconductor position-sensitive device, the silicon microstrip sensor, has been widely used in elementary-particle-physics experiments. To date, the foremost radiation environment has been the large hadron collider (LHC) [1]. In the future, the LHC will be upgraded to the super LHC (SLHC), which will result in an increase in instantaneous luminosity that is 10 times that of the LHC, i.e. increase to 10^{35} cm^{-2} s^{-1}, and an integrated luminosity 5 times that of the LHC, i.e. increase to 3000 fb^{-1}. Radiation-tolerant silicon microstrip sensors will then face the new challenge of coping with a particle fluence of about 1×10^{15} 1-MeV neutron equivalent/cm^2 at a radius of 30 cm from the beamline.

With the radiation damage in silicon, full or over-depletion of ~300 μm thick silicon is unlikely even if the applied bias voltage is high, e.g. 500 V. The aim of the research and development of radiation-tolerant silicon microstrip sensors for the SLHC is to utilize a non-inverting material, a p-type wafer, and to read signals out from the p–n junction side, the n^+-implant strips, the so-called 'n-in-p' sensor [2,3]. Because a high voltage is required towards the end of life of the sensor in order to cope with radiation damage, the proof for the high voltage, e.g. up to 1000 V implicit in design, is required not only to secure a safety margin for any degradation of the breakdown voltage after irradiation, but also to ensure the high quality of the fabrication of sensors and in verifying the detector system to meet the system specifications upon completion.

In an n-in-p sensor, the fixed and the trap charges in the Si–SiO_2 interface, being predominantly positive, create an inversion layer on the n-side. An isolation structure is therefore required to overcome this layer. During high-voltage operation, a sudden increase in leakage current, called microdischarge, occurs at positions where the electric field strength exceeds silicon's avalanche breakdown field strength of ~300 kV/cm. Such a hot spot in an n-in-p sensor is shown in Fig. 1. Optimization of the surface structures in order to reduce the associated electric field in silicon becomes more critical in the n-in-p sensor for the SLHC.

Studies on n-side isolation in n-bulk wafers have been conducted in the past [4–8], and those in p-bulk wafers have been conducted recently, in order to compare the isolation techniques of p-stop, p-spray, and moderated p-spray (or equivalently, of p-stop+p-spray) structures [9,10]. The study described in this paper is a systematic evaluation of the geometries of p-stop structures, conducted in order to gain insight into their electric fields and to provide a guideline for achieving very-high-voltage operation. Other factors such as strip isolation and signal-to-noise ratio were beyond the scope of this study.

2. Technology CAD simulation

The semiconductor industry has developed sophisticated programs called 'technology CAD (or TCAD)' to simulate various processes and devices, a field that was pioneered by Dutton et al. [11]. Though the program is capable of 3D simulations, we used

* Corresponding author. Tel: +81 29 864 5791; fax: +81 29 864 2580.
E-mail address: yoshinobu.unno@kek.jp (Y. Unno).

0168-9002/$ - see front matter © 2010 Elsevier B.V. All rights reserved.
doi:10.1016/j.nima.2010.04.095

the TCAD program ENEXSS/TiSSiEN [12] to simulate a device in two dimensions (2D), which resulted in simplicity that was sufficient to elucidate the relative differences we explored. A simplified surface geometry of p-stop structures is shown in Fig. 2 for (a) a common p-stop, (b) an individual p-stop, and (c) a combined p-stop structure, that were abstracted from Refs. [3,6–8]. Simulations were performed for the cross-section between the two n^+-strips. These three geometries describe the cases in which there are one, two, and three p-stop sections between the n^+-strips. The cross-sectional geometry model is shown in Fig. 3. An example of electric field strength E (V/cm) is shown in Fig. 4. In next sections, electric field distributions near the surface are measured at a depth of $-1.3\,\mu m$ where the electric field is the strongest at the corner of n-strips and p-stops, in order to show the relative differences.

The default values for the input simulation parameters are summarized in Table 1. These values are used throughout the simulations unless otherwise mentioned. An interface trap charge of $1\times10^{11}\,cm^{-2}$ is the default, except in selected simulations in which a charge of $1\times10^{12}\,cm^{-2}$ is considered. The former charge value is a typical of the ⟨1 0 0⟩ orientation [13], and the latter is typical in the case of ionizing radiation [14]. The concentration of the p-stop of $4\times10^{12}\,cm^{-2}$ is taken as a representative value and is a factor that is twice as dense as that used in the case of the p-spray in Ref. [3]. A backplane bias of -200 V that was chosen was considered sufficient to deplete the n-side and to evaluate the relative differences among p-stop structures. The surface of the SiO_2 passivation is floating.

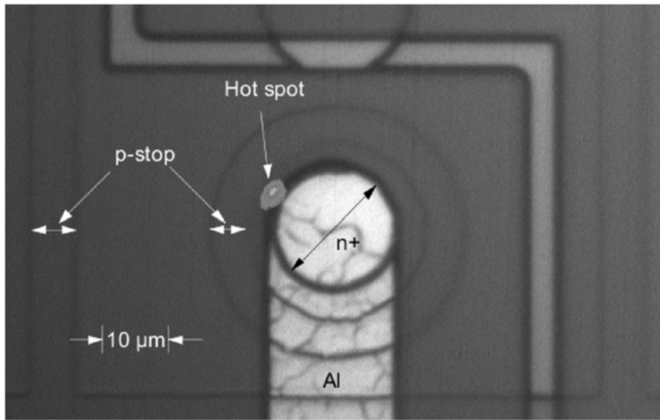

Fig. 1. Hot spot of microdischarge observed in an n-in-p sensor by an infrared camera. The spot is at the edge of the n^+ electrode.

2.1. Common p-stop

The electric field strength E (V/cm) distribution near the surface is shown in Fig. 5 for a common p-stop structure in which the p-stop is 6 μm wide with an interface trap charge of $1\times10^{11}\,cm^{-2}$ (the legend 1e11) and $1\times10^{12}\,cm^{-2}$ (1e12). Although position of the peak moves from the edge of the n^+-strip to the p-stop with

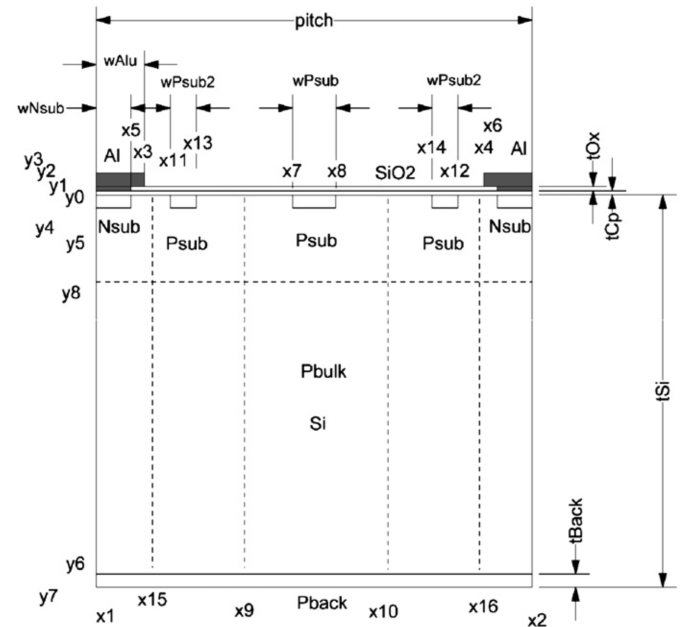

Fig. 3. 2D model of p-stop structures in TCAD simulation. The number and position of p-stops are shown for the analyzed p-stop structures.

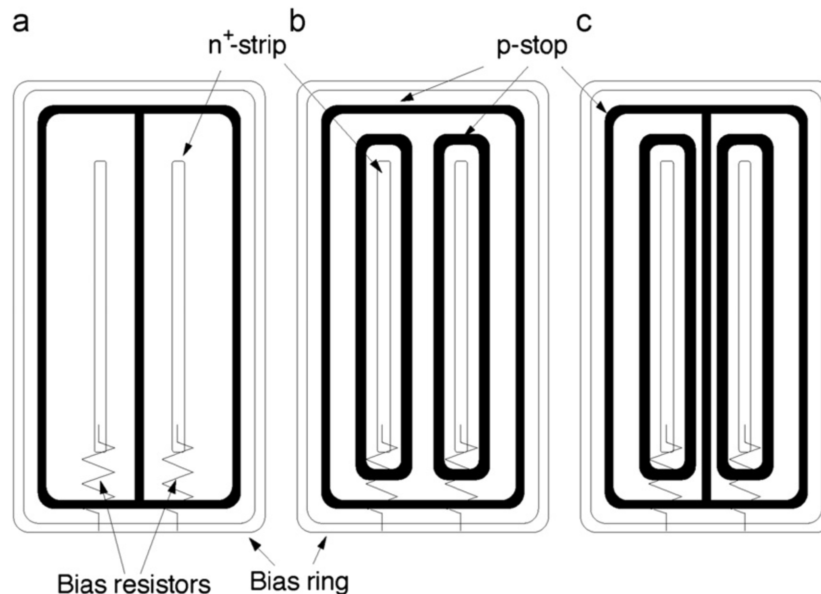

Fig. 2. Simplified schematics of p-stop structures: (a) common p-stop, (b) individual p-stop, and (c) combined p-stop. One, two, and three p-stop sections exist between the n^+ strips.

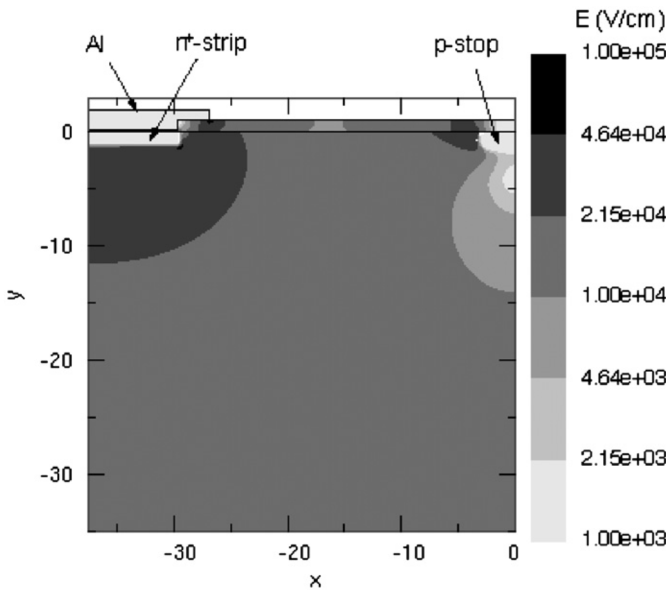

Fig. 4. 2D plot of electric field strength E in the common p-stop structure. The x coordinate is between the n^+-strip and the p-stop. The bias voltage condition is 0 V in the n^+-strips and -200 V in the backplane. High electric fields are at the edges of the n^+-strip and p-stop.

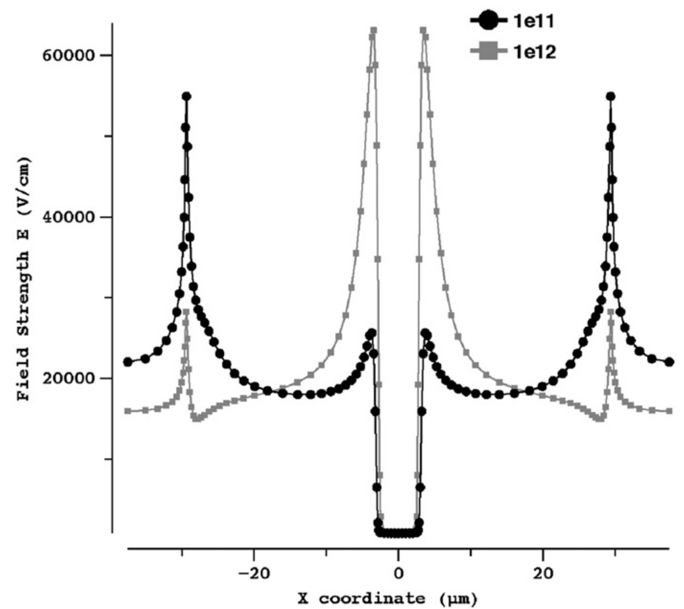

Fig. 5. Electric field strength E in a common p-stop structure with a 6 µm wide p-stop, with interface trap charges of 1×10^{11} cm^{-2} (1e11) and 1×10^{12} cm^{-2} (1e12).

Table 1
Simulation input parameters.

Symbol	Item	Default value
Pbulk	Bulk material	p-type: 4.7×10^{12} cm^{-3} (Resistivity: 3 kΩ cm)
tSi	Bulk thickness	320 µm (Full depletion: 365 V)
Nsub	n^+-strip material	n-type: 1×10^{14} cm^{-2}
wNsub	n^+-strip width (half)	8 µm
tNsub	n^+-strip thickness (depth+smear)	0.9+0.1 µm
wAl	Al electrode width (half)	11 µm
tAl	Al electrode thickness	1.8 µm
tCp	AC coupling material and thickness	SiO_2: 0.2 µm
tOx	Passivation material and thickness	SiO_2: 0.8 µm
Psub	p-stop material	p-type: 4×10^{12} cm^{-2}
wPsub	p-stop width	6 µm
tPsub	p-stop thickness (depth+smear)	0.5+0.5 µm
Pback	Backplane material	p-type: 1×10^{14} cm^{-2}
tPback	Backplane thickness	5 µm
Qit	Si–SiO_2 interface trap charges	Positive: 1×10^{11} cm^{-2}
V(n^+-strip)	Voltage of n^+-strip	0 V
V(Al)	Voltage of Al metal	0 V
V(Backplane)	Voltage of backplane	-200 V

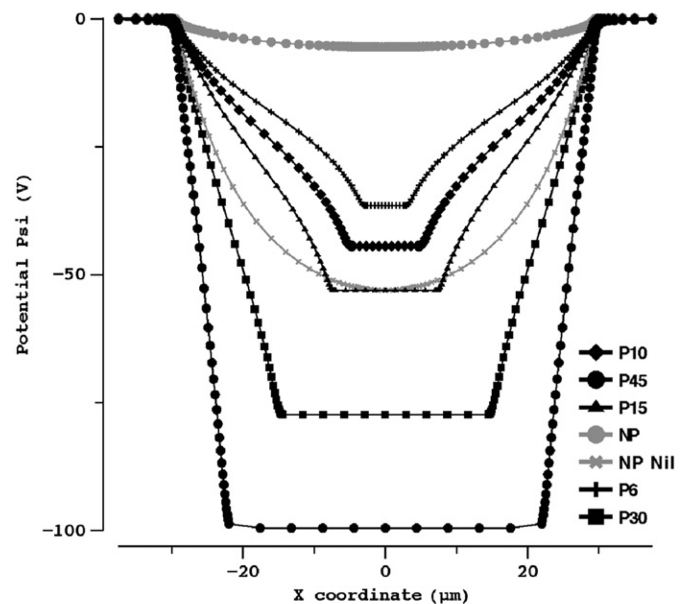

Fig. 6. Electric potential Psi near the silicon surface between n^+-strips in common p-stop structures with p-stop widths of 6–45 µm (P6–P45), together with references without p-stop and with interface trap charges of 1×10^{11} cm^{-2} (NP) and nil (NP Nil).

increasing interface trap charge, the dependence of the two peak values on other parameters, e.g. the p-stop width, is similar, as can be seen in Section 2.6 (Fig. 13).

The electric potential Psi (V) is shown in Fig. 6 for p-stop widths of 6, 10, 15, 30, and 45 µm (legends P6, P10, P15, P30, and P45, respectively), together with no p-stop and a nil (NP Nil) or 1×10^{11} cm^{-2} interface trap charge (NP). With no p-stop and an interface trap charge of 1×10^{11}, the Psi is nearly flat, as expected, due to the conduction in the inversion layer. With no p-stop and nil interface trap charge, the Psi drops to -50 V at the centre between the n^+-strips. This is the potential distribution in the ideal case, i.e. the reference. As the width of the p-stop increases, Psi drops more steeply, to about -100 V at 45 µm. The Psi value vertically across depth (y) is shown in Fig. 7. The interface trap charges of 1×10^{11} and 1×10^{12} cause no noticeable difference in the potential of the p-stops. The electric field strength E is basically governed by this potential Psi and its activity in different situations is summarized in Section 2.6 (Fig. 13).

2.2. Individual p-stop

The idea behind making the potential of the p-stop shallower is to split the p-stop, thus creating a single ring of p-stops around

the n$^+$-strips. Two p-stops, each with a width of 6 μm, are placed between the n$^+$-strips. The potentials for four cases are shown in Fig. 8: <P18>, in which the two p-stops are separated by 6 μm, making the outer-edge-to-outer-edge distance between the two p-stops equivalent to that of a common p-stop with a width of 18 μm; <P30>, in which they are separated by 24 μm and a width of 30 μm; <P45>, in which they are separated by 33 μm and a width of 45 μm; and <P53>, in which they are separated by 41 μm and a width of 53 μm. The potential of the two p-stops becomes deeper as the separation widens and approaches an equivalent width of 45 μm; the potential does not follow the potential distribution of the reference. The potential of the p-stops is shallower than that of common p-stops of equivalent width. The potential, however, is deeper than that of common p-stops of the width narrower than 15 μm.

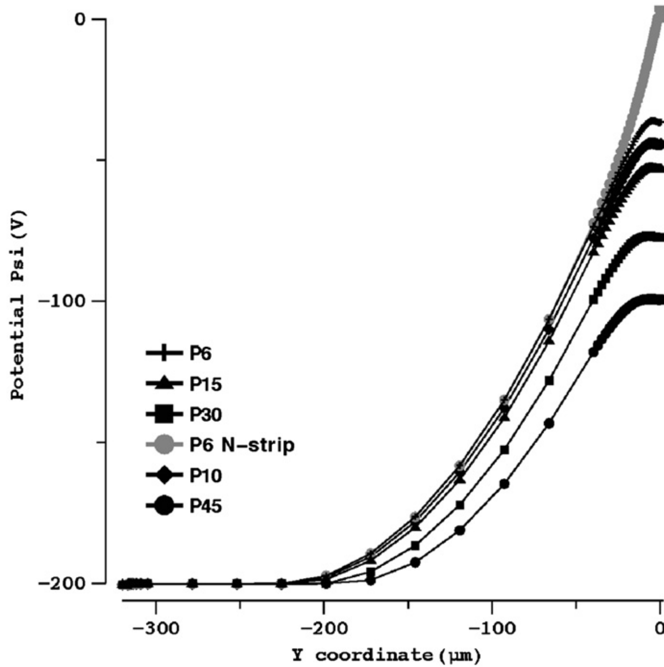

Fig. 7. Electric potential Psi charted vertically through silicon in common p-stop structures with p-stop widths of 6–45 μm at the centre between the n$^+$-strips (P6–P45), and at the n$^+$-strip (P6 N-strip).

2.3. Combined p-stop

A mixture of the common and individual p-stop yields the combined p-stop. In this case, three p-stops exist between the n$^+$-strips. The electric potential Psi is shown in Fig. 9 for these three cases: for the legend <P30>, the outer-edge-to-outer-edge distance between the three p-stops is equivalent to a common p-stop with a width of 30 μm, for <P45>, it is equivalent to 45 μm, and for <P53>, it is equivalent to 54 μm. The potential of the outer two p-stops is dragged to the one at the centre, although it is slightly shallower as the separation from the centre widens. The potential is deeper than that of the equivalent width in the case of an individual p-stop.

2.4. P-stop in an asymmetric position

The position of the p-stop between the n$^+$-strips is varied to simulate the asymmetric placement of the p-stop. The case of a common p-stop that is 6 μm wide is considered. The electric potential Psi is shown in Fig. 10 for the following cases: P6 for the case of symmetric placement; <P18>, in which the nearest edge of the p-stop to the n$^+$-strip is equivalent to a common p-stop with a width of 18 μm; <P30>, in which it is equivalent to 30 μm; and <P45>, in which it is equivalent to 45 μm. The potential of the p-stop has only weak dependence on the location.

2.5. Strip pitch

Another factor in the design of a microstrip sensor is the pitch of the strips. For a p-stop structure, two main criteria can be thought: (1) to maintain the width of the p-stop constant or (2) to maintain the ratio of the width of the p-stop to the strip pitch

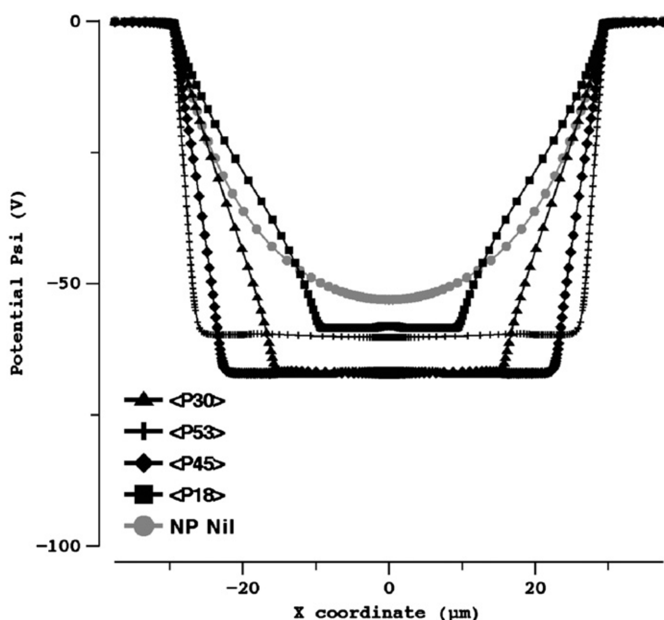

Fig. 8. Electric potential Psi in individual p-stop structures with outer-edge-to-outer-edge distances between the two p-stops being 18–53 μm (<P18> to <P53>) and the reference (NP Nil).

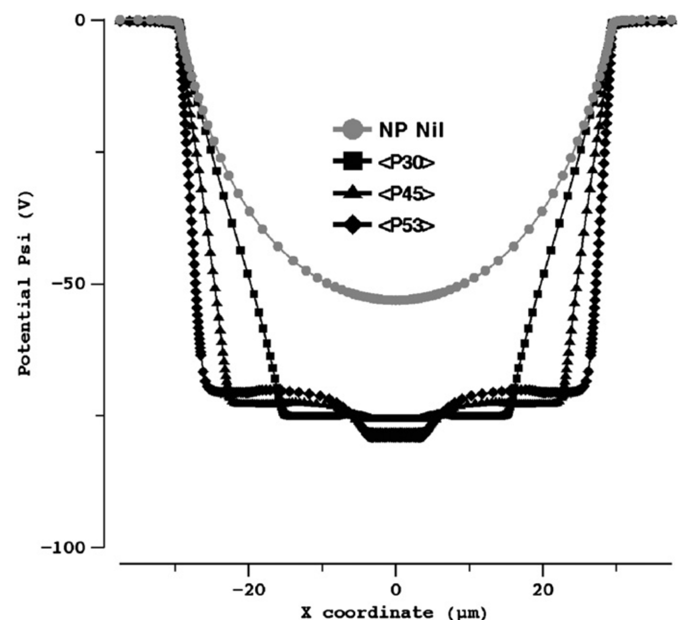

Fig. 9. Electric potential Psi in combined p-stop structures with the outer-edge-to-outer-edge distance between the three p-stops being 30–53 μm (<P30> to <P53>) and the reference (NP Nil).

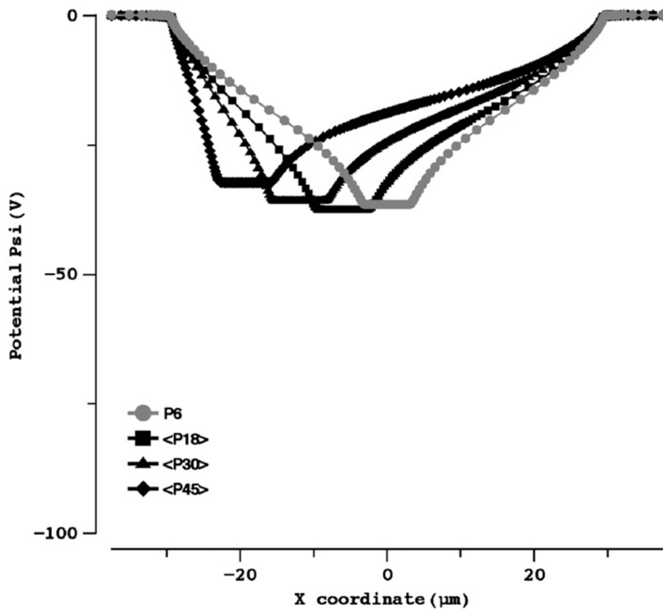

Fig. 10. Electric potential Psi of asymmetric positions of 6 μm wide p-stops in common p-stop structures, with the minimum distance between the n⁺-strip and the p-stop equivalent to a p-stop width of 18–45 μm (<P18> to <P45>).

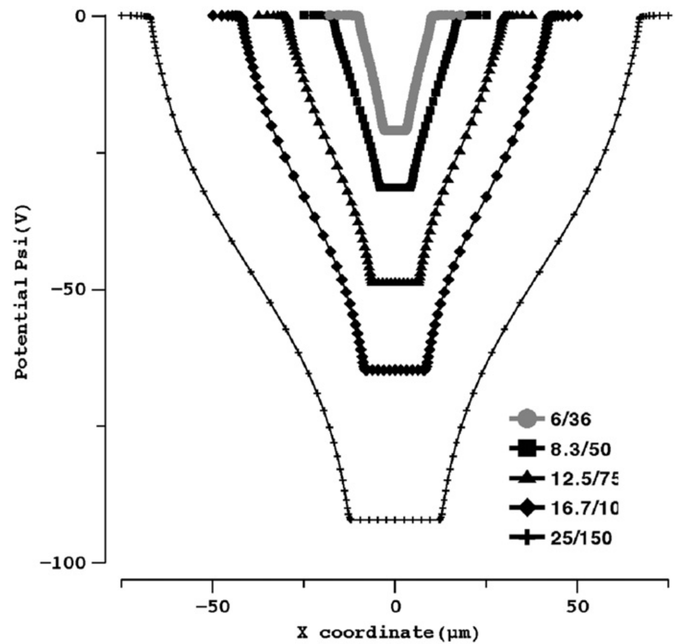

Fig. 12. Electric potential Psi in common p-stop structures with a constant width/pitch ratio (W/P) of 1/6 and strip pitches of 36–150 μm.

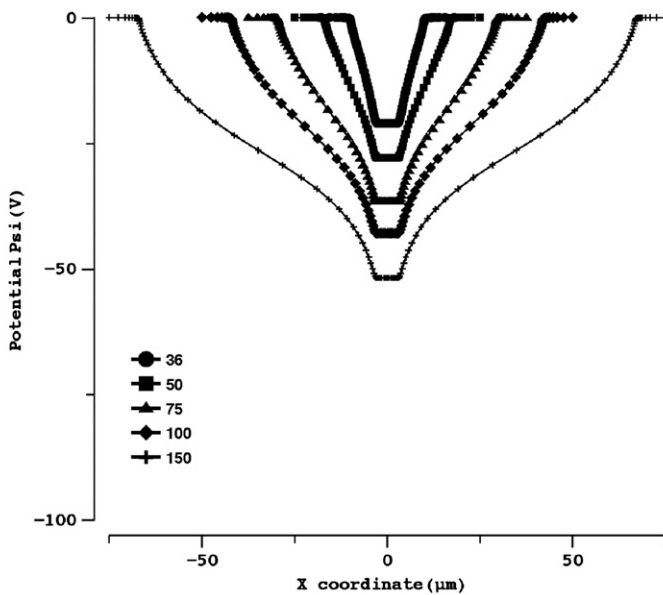

Fig. 11. Electric potential Psi, in common p-stop structures with a constant p-stop width of 6 μm and strip pitches of 36–150 μm.

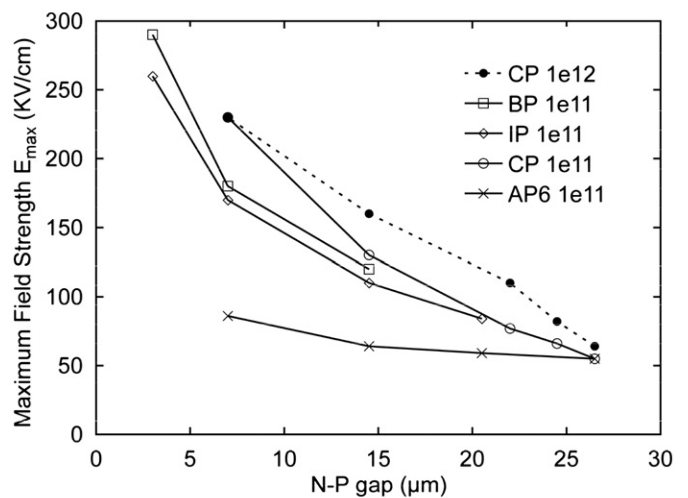

Fig. 13. Maximum electric field strength E_{max} vs. minimum distance between the n⁺-strip and the p-stop, N–P gap of common p-stop structures with interface trap charges of 1×10^{11} cm^{-2} (CP 1e11) and 1×10^{12} cm^{-2} (CP 1e12), individual p-stop (IP 1e11), combined p-stop (BP 1e11), and asymmetric position of common p-stop (AP6 1e11).

constant. The electric potential Psi in the common p-stop structure for the case of a constant width of 6 μm is shown in Fig. 11 with strip pitches of 36, 50, 75, 100, and 150 μm, and in Fig. 12 for the case of a constant ratio of 1:6. The potential of the p-stops deepens as the pitch widens, and it becomes even deeper in the case of the constant ratio, because the p-stop width widens with widening pitch.

2.6. Maximum electric field strength

The electric potential of the p-stops plays a fundamental role. The distribution of potential defines the electric field and the maximum electric field strength E_{max} (V/cm) at the edges of the n⁺-strips and p-stops, which are best known from the TCAD simulations. The maximum electric field strength E_{max} is summarized as a function of the gap between the n⁺-strip and the nearest p-stop, which is denoted as N–P gap in Fig. 13 for the various p-stop structures and in Fig. 14 for the strip pitches. These dependences provide a guideline for the design of an n-in-p sensor with p-stop structures for very-high-voltage operation. E_{max} can be reduced as the positioning of the p-stops becomes more symmetric, the p-stop width narrows, and the N–P gap widens, even with multiple p-stops. Although the absolute value of E_{max} should be regarded as qualitative, a relative E_{max} value provides a quantitative measure as a guideline.

The case of Fig. 2 corresponds to a combined p-stop structure with an N–P gap of about 3 μm along the horizontal cross-section.

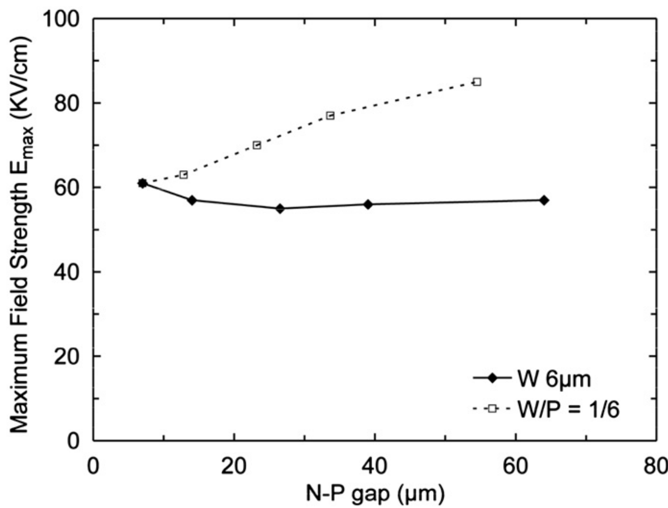

Fig. 14. Maximum electric field strength E_{max} vs. minimum distance between the n^+-strip and the p-stop, N–P gap of common p-stop structures with a constant-width p-stop (W 6 μm) and constant W/P of 1/6.

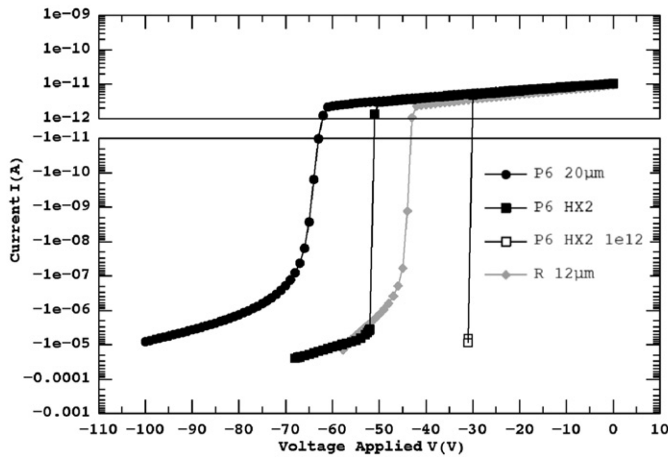

Fig. 15. Dynamic change of resistance between n^+-strip and bias-ring (n^+) in the punch-through protection (PTP) structure with p-stop width of 6 μm and n^+–n^+ distance of 20 μm (P6 20 μm), PTP structure with the extended Al electrode (p6 HX2), PTP structure with the extended Al electrode and with the interface trap charge of 1×10^{12} cm^{-2} (P6 HX2 1e12), and PTP structure with p-spray of the n^+–n^+ distance of 12 μm (R 12 μm).

The onset of the microdischarge occurred at around 400 V. In Fig. 13 E_{max} is ~300 kV/cm, which is almost equal to the avalanche breakdown field strength at a bias voltage of 200 V. By enlarging the N–P gap to 15 μm, e.g., E_{max} is reduced to <150 kV/cm. The distance of the N–P gap must be balanced with the onset voltage of the punch-through that is larger for the larger N–P gap. A new fabrication process that employs a modified mask with the N–P gap of 7 μm has successfully pushed the onset of microdischarge above 1000 V [3].

If a conductive layer on top of the passivation layer exits, it works like a field plate of the n-strip potential and reduces the electric field at the n-strip and enhances at the p-stop edges. The dependence on the N–P gap of the electric fields at those edges follows the same trend as in the above.

2.7. Punch-through protection structure

Protection against a situation in which the voltage of the n^+-strips drops below the breakdown voltage of the AC coupling insulator of about 100 V is provided by a punch-through protection (PTP) structure. This structure is a narrow gap between the bias-ring (n^+) and the end of the n^+-strips. The voltage of the n^+-strips drops when a large current passes through the bias resistor from a splash of charge particles into the silicon sensor, e.g. due to mishandling of the beam.

A PTP structure in an n-in-p microstrip sensor is analyzed for the gap between the bias-ring (n^+) and the end of the n^+-strips, an N–N gap of 20 μm with a p-stop that is 6 μm wide at the centre (P6 20 μm). Variations in the structure are those with an extended aluminium electrode of the bias-ring (n^+) over the entire area of the p-stop (P6 HX2) proposed in this paper and with an interface trap charge of 1×10^{12} cm^{-2} (P6 HX2 1e12). For a comparison, analyzed is the PTP with the p-spray of 2×10^{12} cm^{-2} with the

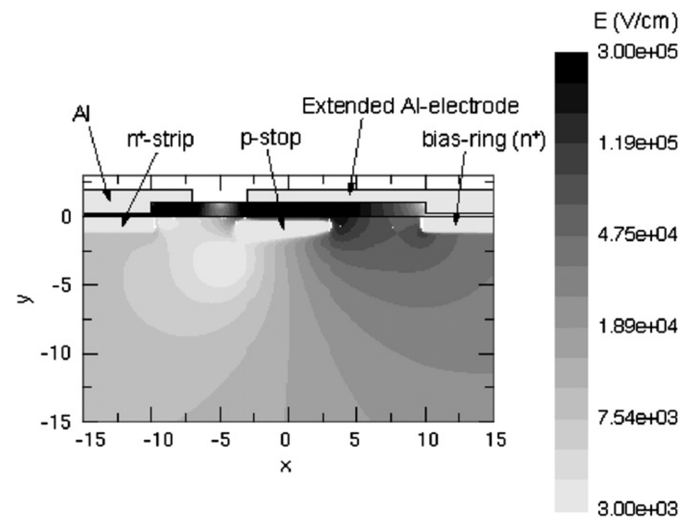

Fig. 16. Electric field strength E in PTP structure of p-stop with an extended Al electrode, with applied voltage of −50 V in the n^+-strip, applied voltage of 0 V in the bias-ring, and applied voltage of −200 V in the backplane.

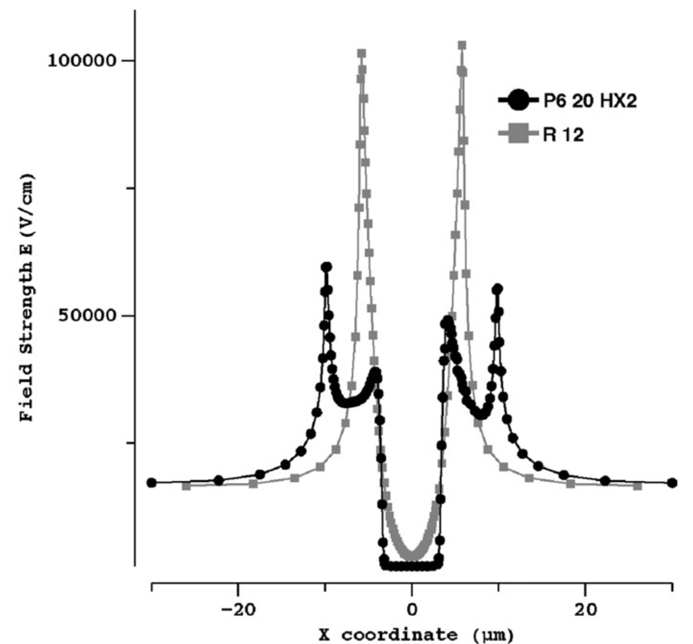

Fig. 17. Electric field strength E in PTP structures of p-stop with an extended Al electrode and an n^+-strip and bias-ring (n^+) distance of 20 μm (P6 20 HX2) and of p-spray with a distance of 12 μm (R 12), under normal conditions of 0 V in both the n^+-strip and the bias-ring.

N–N gap of 12 μm. The resistance for the N–N gap is shown in Fig. 15. An example of the electric field strength E of the PTP structure (P6 HX2) is shown in Fig. 16 for a voltage of 50 V for an n^+-strip when the PTP is on. Addition of the extended electrode helps to reduce the onset voltage of the p-stop with N–N gap of 20 μm nearly equivalent to the p-spray of 12 μm. The onset voltage is rather sensitive to the interface trap charges, and should therefore be regarded as only a qualitative measure. The trend, however, persists.

The electric field strength E is shown in Fig. 17 under the normal condition of both the n^+-strip and the bias-ring (n^+) at 0 V. The maximum electric field strength E_{max} is in the range of 60–150 kV/cm, which would still be safe for high-voltage operation.

3. Summary

A novel radiation-tolerant silicon microstrip sensor developed for the SLHC uses a non-inverting silicon material, a p-type wafer and to read signals out from the n^+-strips. In n-in-p silicon sensors, a n^+-strip isolation structure with a p-type impurity is required in the surface of silicon in order to cope with the inversion layer formed by the positive trap charges at the Si–SiO_2 interface. Three cases of p-stop structures – common, individual, and combined – are systematically analyzed in terms of width and position of the p-stops.

Three dynamics are quantitatively investigated: the dependence of the electric potential of the p-stops on the width of the p-stops, the similarity between the electric potential of multiple p-stops which therefore function more like a single large p-stop, and the correlation between the electric potential of the p-stops and the electric field strength in various configurations. The distribution of electric potential defines the maximum electric field strength E_{max} at the edge of the n^+-strips and the p-stops, which is best understood from the TCAD simulations.

The dependence of E_{max} on the gap between the n^+-strip and the p-stop, i.e. the N–P gap provides a guideline for the design of an n-in-p sensor with p-stop structures for very-high-voltage operation. E_{max} can be reduced as the positioning of the p-stops becomes more symmetric, the p-stop width narrows, and the N–P gap widens, even with multiple p-stops. Although the absolute value of E_{max} may yet be qualitative, the relative E_{max} value provides a quantitative measure as a guideline. An example of fabrication has demonstrated the usefulness of this guideline.

Acknowledgments

We would like to express our thanks to the detector development program of KEK for use of the TCAD program. This research was partly supported by the Japan Grant-in-Aid for Scientific Research (A) (Grant no. 20244038), Research (C) (Grant no. 20540291) and Research on Priority Area (Grant no. 20025007).

References

[1] A. Ahmad, et al., Nucl. Instr. and Meth. A 578 (2007) 98.
[2] H.F.-W. Sadrozinski et al., Development of non-inverting silicon strip detectors for the ATLAS ID upgrade. Available at: https://edms.cern.ch/file/816759/1/ATLAS_RD_SSD_May_18_06.doc.
[3] Y. Unno, Development of n-on-p silicon sensors for very high radiation environment, Nucl. Instr. and Meth., this issue, doi:10.1016/j.nima.2010.04.080.
[4] J. Matheson, et al., Nucl. Instr. and Meth. A 362 (1995) 297.
[5] R.H. Richter, et al., Nucl. Instr. and Meth. A 337 (1996) 412.
[6] P.I. Hopman, et al., Nucl. Instr. and Meth. A 383 (1996) 98.
[7] Y. Iwata, et al., IEEE Trans. Nucl. Sci. NS-45 (1998) 303.
[8] Y. Unno, et al., IEEE Trans. Nucl. Sci. NS-45 (1998) 401.
[9] C. Piemonte, IEEE Trans. Nucl. Sci. NS-53 (2006) 1694.
[10] G. Pellegrini, et al., Nucl. Instr. and Meth. A 579 (2007) 599.
[11] Stanford Technology CAD home page. Available at: http://www-tcad.stanford.edu/tcad.html.
[12] ENEXSS/TiSSiEN, TCAD International Inc. Available at: http://www.tcad-international.com/english/product/index.html.
[13] S.M. Sze, in: Physics of Semiconductor Devices, second ed., Wiley-Interscience, 1981 386pp.
[14] H.F.-W. Sadrozinski, et al., Nucl. Instr. and Meth. A 579 (2007) 769.